







Inter-Turn Fault Diagnosis of Induction Motor Using a Root-Prony and Fuzzy Logic Method

¹Faculty of Applied Sciences, Ibn Khaldoun University of Tiaret Algeria, Tiaret, Algeria | ²Autonex Systems Limited, London, UK | ³School of Electrical and Electronic Engineering, The University of Sheffield, UK | ⁴Department of Electrical Engineering, National Kaohsiung University of Science and Technology, Kaohsiung City, Taiwan | ⁵University of Brest, UMR CNRS 6027 IRDL, Brest, France | ⁶Huanjiang Laboratory, Zhejiang University, Zhuji, China | ⁷Center for Research on Microgrids (CROM), AAU Energy, Aalborg University, Aalborg, Denmark

Correspondence: Hafiz Ahmed (hafiz.h.ahmed@ieee.org)

Received: 14 June 2025 | Revised: 17 September 2025 | Accepted: 29 October 2025

Handling Editor: Akhil Garg

Keywords: fault diagnosis | fault severity index | fuzzy control | induction motor | inter-turn fault | real-time fault detection

ABSTRACT

This paper proposes a novel diagnostic approach for detecting inter-turn short-circuit faults in induction motors, combining the root-Prony method with fuzzy logic. Traditional techniques, such as the periodogram, have limitations in detecting lowmagnitude harmonics and providing high-frequency resolution. To address these challenges, complex high-resolution methods, such as MUSIC and ESPRIT, have been developed. In this study, the root-Prony method is selected for its adaptability and low computational burden as it does not rely on space decomposition, making it faster than MUSIC. The proposed approach focuses on analysing the stator current signal within a specific frequency range near the fundamental rotor slot harmonics. By reducing the number of processed samples, computation time is further decreased. The integration of fuzzy logic enables intelligent decision-making regarding the condition of the stator circuit by considering harmonic magnitudes under different load torque values for accurate diagnosis. Experimental tests were conducted on an induction motor initially powered directly from an electrical network supplying symmetrical sinusoidal three-phase voltages. To demonstrate the robustness of the proposed method in noisy environments, additional tests were performed with the motor powered by a converter. In such scenarios, the conventional periodogram-based technique was unable to detect the desired harmonics due to the high harmonic content in the stator current signals. The test results confirm the superior effectiveness of the root-Prony method over the classical periodogram technique in estimating the frequencies and amplitudes of the targeted harmonics. The integration of the root-Prony method with fuzzy logic offers an advanced, efficient and reliable solution for fault diagnosis in induction motors.

1 | Introduction

The diagnosis of stator short circuit fault in induction motors (IMs) remains a significant industrial concern due to the deterioration of stator winding insulation [1]. Moreover, the application area and operating environment of IMs considerably influence the occurrence of such faults. According to ref [2], stator faults

account for approximately 9% of total failures in low-voltage IMs, rising to 35%–40% in medium-voltage IMs, and exceeding 65% in high-voltage machines. Additionally, as reported in ref. [3], stator winding faults represent the predominant failure mode in large alternating current (AC) motors, accounting for nearly 60% of cases. Specifically, inter-turn short circuit (ITSC) constitute around 26% of all stator-related faults [4].

This is an open access article under the terms of the Creative Commons Attribution License, which permits use, distribution and reproduction in any medium, provided the original work is properly cited.

© 2025 The Author(s). IET Collaborative Intelligent Manufacturing published by John Wiley & Sons Ltd on behalf of The Institution of Engineering and Technology.

It is important to note that the insulation quality is typically the most critical factor affecting the longevity and reliability of electrical machine windings. Although the insulation system is generally designed for a service life of 25-30 years [5], it is highly susceptible to ageing and temperature variations, which are primary contributors to stator winding failures. In this context, motor current signature analysis (MCSA) has become one of the most widely used techniques for diagnosing ITSC faults [6]. This method identifies frequency components characteristic of such faults through power spectral density (PSD) estimation, often using the periodogram technique [7], valued in industry for its simplicity and rapid computation. However, the periodogram offers limited frequency resolution and struggles to detect low-amplitude harmonics [8]. These conventional methods show their limitations when load variations occur. In such cases, the signals become nonstationary and therefore require the use of more suitable approaches, such as timefrequency or time-scale methods. Among them, the short-time Fourier transform (STFT) is the most commonly employed, as it allows tracking the temporal evolution of the signal's frequency components, for instance during speed variations. However, its main drawback lies in the trade-off between time and frequency resolution, which restricts its ability to detect low-amplitude harmonics that characterise early stages of ITSC faults [9]. Furthermore, using a rotating reference frame, such as the Park transformation, can mask low-amplitude fault signatures by shifting them to very low frequencies, which further complicates their detection [10].

This limitation has driven the development of several highresolution spectral estimation methods [11], which rely on parametric signal models and decompose the signal space into signal and noise subspaces. Among these, techniques, such as MUSIC (multiple signal classification) [12], ESPRIT (estimation of signal parameters via rotational invariance techniques) [13], and the matrix pencil method [14, 15], are well regarded for their noise resilience and high frequency resolution with short data window requirements. Nevertheless, their algorithmic complexity results in increased computation time. To address this, various adaptations, such as zoom-MUSIC [11] and root-MUSIC [8], have been introduced to reduce computational demands. Table 1 presents a qualitative comparison of commonly used fault detection techniques. This comparison focuses on key performance aspects such as frequency resolution, noise robustness, computational cost and algorithmic complexity.

As seen in Table 1, the periodogram offers low computational cost but suffers from poor frequency resolution and low sensitivity to noise, making it unsuitable for detecting low-amplitude

harmonics. High-resolution methods, such as MUSIC and ESPRIT, achieve excellent accuracy but at the cost of high complexity and processing time. Root-MUSIC slightly reduces the computational burden but still requires subspace decomposition. The matrix pencil method, in its simplified form, emerges as a competitive alternative. It offers high frequency resolution and strong robustness to noise by relying on a singular value decomposition (SVD) framework. Although the algorithm remains moderately complex, the optimisation strategies, such as focusing on a specific harmonic component, can significantly reduce computation time. This makes matrix pencil particularly well-suited for detecting fault-related harmonics in noisy environments, without the need for subspace partitioning as in MUSIC or ESPRIT.

Motivated by the qualitative performance comparison, we are proposing root-Prony method, which provides a good balance between resolution and complexity. It achieves accurate harmonic detection within a narrow frequency band while significantly reducing computation time, making it particularly suitable for fast diagnostic tasks. For example, it can effectively diagnose ITSC faults in IM stator windings under varying load torque conditions using the parametric root-Prony method as demonstrated in refs. [16-18]. This method is particularly suitable for analysing stator current signals, which can be represented as a linear combination of time-invariant sinusoidal components [16-18]. Furthermore, root-Prony offers high frequency resolution and faster execution compared to MUSIC and ESPRIT as it does not require signal space decomposition [16-18]. Although slightly more sensitive to noise than these methods, root-Prony maintains a significantly shorter computation time relative to conventional techniques. To address residual challenges, the proposed strategy involves analysing the stator current signal within a targeted frequency band, specifically around the fundamental rotor slot harmonic frequencies, where the ITSC fault signature is expected to appear. This focused analysis helps prevent confusion with unrelated lowfrequency signatures from external sources [16-18], while reducing the number of processed samples and further decreasing computation time. Additionally, rather than estimating the number of harmonics, this approach predefines them, simplifying the analysis.

The primary objective of this research is to estimate the frequencies and amplitudes of fault-related harmonics for various load torque conditions. Initially, the periodogram-based digital signal processing (DSP) method was applied, given its widespread use in industrial diagnostics. However, it proved inadequate in detecting the low-amplitude harmonics indicative of

 $\textbf{TABLE 1} \quad | \quad \text{Qualitative comparison of fault detection methods}.$

Method	Frequency resolution	Noise robustness	Computation time	Complexity	Requires signal model?
Periodogram	Low	Low	Very low	Low	No
MUSIC	Very high	High	High	High	Yes
ESPRIT	Very high	High	High	High	Yes
Root-MUSIC	Very high	Medium to high	Medium	Medium	Yes
Matrix pencil	High	Medium to high	Low to medium	Medium	Yes
Root-Prony	High	Medium	Low	Medium	Yes (sinusoidal mode)

ITSC faults. Consequently, the root-Prony method was adopted and demonstrated superior performance in comparison. Moreover, to enhance diagnostic decision-making, the root-Prony method was combined with a fuzzy logic-based artificial intelligence system. A fuzzy inference model was developed using the harmonic magnitudes and corresponding load torque values as input variables, enabling the classification of the motor's stator condition through linguistic reasoning and membership degree evaluation within fuzzy sets.

It is also essential to consider that, besides stator ITSC faults, factors, such as power supply voltage asymmetry or nonsinusoidal voltage waveforms, can generate harmonics at frequencies coinciding with those produced by ITSC faults [19, 20]. Without accounting for the power supply condition, misinterpretation of the diagnostic results could occur. Therefore, to validate the proposed method, experimental tests were conducted on an induction motor initially powered by a symmetrical sinusoidal three-phase supply. To assess robustness in noisy conditions, additional tests were performed with the motor fed by a converter at various supply frequencies. Under these circumstances, the conventional periodogram-based technique failed to detect the desired fault harmonics due to the increased harmonic content introduced by the modulation process. In contrast, the root-Prony method successfully identified the fault characteristics. The experimental results confirm the effectiveness of the proposed diagnostic approach, demonstrating its capability to accurately detect and assess the severity of stator winding ITSC faults in induction motors.

Summary of the main contributions: Firstly, this work develops an improved root-Prony method, optimised for precise extraction of rotor slot harmonics by incorporating targeted frequency band selection, thereby reducing computation time without sacrificing accuracy. Secondly, it introduces a fuzzy logic-based classification system to evaluate fault severity under varying load conditions, using harmonic magnitudes as decision variables, enabling rule-based and interpretable diagnostics. Thirdly, the combined method is implemented and experimentally validated on a customised test bench, demonstrating effectiveness under both ideal and realistic (noisy and inverterfed) operating conditions. Finally, the study proves the robustness and practical applicability of the proposed approach, particularly in detecting low-amplitude fault signatures, a scenario where conventional diagnostic methods often fail.

The remainder of this article is organised as follows: Section 2 discusses the frequency signature of ITSC faults in IMs. The conventional root-Prony method and its improved version are presented in Section 3, whereas the performance of the proposed method is evaluated in Section 4 using a laboratory-scale test setup. Performance enhancement of the proposed method using a fuzzy logic approach is described in Section 5. Finally, Section 6 concludes the article.

2 | Frequency Signatures of ITSC Stator Faults

When a short-circuit fault occurs in the stator winding, it causes changes in the stator currents. In ref. [21], the authors demonstrated that the presence of an ITSC fault results in an

increased current in the affected phase and the generation of harmonics, with frequencies given as follows:

$$f_{\rm sc} = f_s \left[n_{\rm rt} \frac{N_B}{p} (1 - s) \pm 2n_{\rm sa} \pm n_{\rm st} \right],$$
 (1)

where f_s represents the supply frequency, p is the number of pole pairs, N_B is the number of rotor bars and s is the slip. The integers $n_{\rm st}$, $n_{\rm sa}$ and $n_{\rm rt}$ correspond to the stator, saturation and rotor, respectively. However, certain ITSC fault indicators are more conclusive than others. In ref. [22], it was demonstrated that this fault is characterised by an increase in both the fundamental component and the third harmonic. To simplify the subsequent analysis, by ignoring the saturation effect and considering $n_{\rm st} = n_{\rm rt} = 1$, the expression for the first order rotor slot harmonics can be obtained [16, 23]. In this case, the upper rotor slot harmonic (U_RSH) and lower rotor slot harmonic (L_RSH) are defined as follows:

$$f_{\text{U-RSH}} = f_s \left[\frac{N_B}{p} (1 - s) + 1 \right],$$
 (2)

$$f_{\text{L-RSH}} = f_s \left[\frac{N_B}{p} (1 - s) - 1 \right].$$
 (3)

In this study, the saturation term in Equation (1) is deliberately neglected to simplify the harmonic expression and focus on the most relevant fault component, namely, the lower rotor slot harmonic. Previous works [22] have shown that magnetic saturation primarily affects the fundamental component and certain low-order harmonics, while its impact on the L_RSH frequency range remains relatively minor. Therefore this modelling assumption is reasonable for the analysis of ITSC fault signatures, since the variations in L_RSH are mainly governed by the fault and not by magnetic saturation.

Note that, the authors in ref. [24] shows that the impact of the short-circuit fault is more noticeable at the level of the L_RSH than at the U_RSH. Therefore, this study focuses on tracking the L_RSH for the diagnosis of an ITSC fault.

3 | Root-Prony Method: Overview and Improvement

Prony's method is capable of extracting valuable information, namely, frequency, magnitude, phase and damping, from the components of a signal. To apply this method, the signal to be processed must take the form of a complex exponential series or a sum of sinusoids. On the other hand, the stator current signal $i_s(t)$ is simply the sum of N_H undamped sinusoids, including the fundamental component, eccentricity-related harmonics, harmonics produced by the rotor slots, harmonics caused by power supply disturbances and, in the case of faults, additional frequency components that may be created and added to the signal [25]. Therefore, the temporal form of the signal $i_s(t)$ can be represented as follows:

$$i_{s}(t) = \sum_{i=1}^{N_{s}} I_{i} \cos(2\pi f_{i}t + \varphi_{i}), i = 1, ..., N_{s},$$
 (4)

where N_s is the number of sinusoids, and I_i , f_i and ϕ_i represent the amplitude, frequency and phase of the i-th sinusoid, respectively. The signal Equation (4) is in continuous-time whereas measurements are only available in discrete-time. Therefore, discrete-time version of the signal Equation (4) can be written as follows:

$$i_s(n) = \sum_{i=1}^{N_s} I_i \cos\left(2\pi f_i \frac{n}{f_{sf}} + \varphi_i\right), n = 0, 1, ..., N - 1,$$
 (5)

where $f_{\rm sf}$ represents the sampling frequency and N is the number of samples. Using the Euler equation [26], that is

$$\cos\left(2\pi f_i \frac{n}{f_{sf}} + \varphi_i\right) = \frac{1}{2} \left(e^{j\left(2\pi f_i \frac{n}{f_{sf}} + \varphi_i\right)} + e^{-j\left(2\pi f_i \frac{n}{f_{sf}} + \varphi_i\right)} \right),$$

the signal Equation (5) can be rewritten as:

$$i_{s}(n) = \sum_{i=1}^{N_{s}} \frac{I_{i}}{2} e^{j\left(2\pi \frac{f_{i}}{f_{sf}}n + \varphi_{i}\right)} + \sum_{l=1}^{N_{s}} \frac{I_{i}}{2} e^{-j\left(2\pi \frac{f_{i}}{f_{sf}}n + \varphi_{i}\right)}, \tag{6}$$

where $f_{\rm sf}$ retains the same meaning as defined before. Equation (6) is a combination of two complex exponentials. This can be simplified into a single expression using a sum of q complex exponentials, where instead of ranging from 1 to $N_{\rm s}$, the range extends from 1 to q, as follows:

$$i_s(n) = \sum_{i=1}^q \bar{I}_i e^{j\left(2\pi \frac{\bar{f}_i}{f_{sf}}n + \varphi_i\right)},\tag{7}$$

where $\bar{I}_i = \frac{l}{2}$, $\bar{f}_i = f_i$, $\bar{f}_{i+N_s} = -f_i$ for $i = 1, ..., N_s$, $q = 2N_s$ with q being the order of the modelled signal. Note that Equation (7) represents the stator current model in the discrete time domain same as Equation (6).

3.1 | Root-Prony Methods: Step-By-Step Description

The root-Prony method is based on fitting the following model to the discrete-time stator current signal $i_s(n)$ given in Equation (7) as follows:

$$\stackrel{\wedge}{i}_s(n) = \sum_{i=1}^q h_i z_i^{n-1},$$
(8)

$$h_i = \bar{I}_i e^{j\varphi_i}, \tag{9}$$

$$z_i = e^{\left(\alpha_i + j2\pi f_i\right)/f_{\rm sf}},\tag{10}$$

where h_i and z_i are the residuals and discrete poles of the model, α_i is the damping coefficient and q is the number of desired complex exponentials. Note that $h_i \in \mathbb{C}$ and z_i are distinct values and z_i is within the λ with $\lambda = \{z \in \mathbb{C} : |z| \le 1\}$ denoting the unit circle. Then, the signal parameters I_i , f_i , α_i and ϕ_i can be computed by minimising the following prediction error function:

$$\varepsilon(n) = \sum_{n=1}^{N} \left| i_s(n) - \hat{i}_s(n) \right|^2 = \sum_{n=1}^{N} \left| i_s(n) - \sum_{i=1}^{q} h_i z_i^{n-1} \right|^2. \tag{11}$$

Typically, no analytical solution is available for the nonlinear Equation (11); therefore, it is difficult to solve [27]. To address this issue, three steps must be considered to determine the z_i values separately from the h_i values. In this case, to find the roots of a polynomial, a set of linear equations must first be established. Moreover, it is known that Prony's method considers the current signal $\hat{i}_s(n)$, given by Equation (8) as the solution of the following recurrence equation [27, 28]:

$$\hat{i}_{s}(n) = -\sum_{i=1}^{q} a_{i} \hat{i}(n-i), n = 0, 1, ..., N-1.$$
 (12)

• Step-1: determining the coefficients a_i

In this step, to solve Equation (12), it is necessary that $N \gg q$. By applying the criterion of minimising the prediction error in the least squares sense, the resolution of this equation reduces to the covariance method defined in matrix form as follows [28]:

$$A = C^{-1}R, (13)$$

where $A = \begin{bmatrix} a_1 & a_2 & \cdots & a_q \end{bmatrix}^T$ represents the unknown vector to be determined, R is the first line of the matrix C and C is considered the estimated covariance matrix defined by:

$$C_{ij} = \sum_{k=1}^{N-q+1} \hat{i}_{s_{i+k}} \hat{i}_{s_{j+k}}, \tag{14}$$

• Step-2: determining the z_i roots

This step consists of determining the z_i of Equation (8), which allows computing the characteristic polynomial's roots:

$$P(z) = \sum_{i=0}^{q} a_i z^{q-i} = 0,$$
 (15)

with $a_i \in \mathbb{C}$ and $a_0 = 1$. The name root-Prony method is derived from the calculation of the roots of Equation (15). Thus, based on Equation (10), it is possible to calculate the frequencies f_i and the damping coefficients α_i as follows [29]:

$$f_i = \frac{1}{2\pi T_s} t g^{-1} \left[\frac{\operatorname{Im}(z_i)}{\operatorname{Re}(z_i)} \right], f_i \in \mathbb{R},$$
 (16)

$$\alpha_i = \frac{ln|z_i|}{T_s}, \alpha_i \in \mathbb{R}, \tag{17}$$

where the sampling period is given by $T_s = 1/f_{sf}$.

• Step-3: determining the h_i coefficients

Knowing the z_i , the coefficients h_i can be determined using Equation (8), which was developed in matrix form as follows [23]:

$$\begin{bmatrix}
i_{s}(1) \\
i_{s}(2) \\
i_{s}(3) \\
\vdots \\
i_{s}(q)
\end{bmatrix}_{I_{s}} = \begin{bmatrix}
1 & 1 & \dots & 1 \\
z_{1}^{1} & z_{2}^{1} & \dots & z_{q}^{1} \\
z_{1}^{2} & z_{2}^{2} & \dots & z_{q}^{2} \\
\vdots & \vdots & \vdots & \ddots & \vdots \\
z_{1}^{n-1} & z_{2}^{n-1} & \dots & z_{q}^{n-1}
\end{bmatrix}_{I_{s}} \begin{bmatrix}
h_{1} \\
h_{2} \\
h_{3} \\
\vdots \\
h_{q}
\end{bmatrix}_{I_{s}} .$$
(18)

Then, the coefficients h_i can be obtained from Equation (18) as follows:

$$H = Z^{-1}I_{s}. (19)$$

Then by comparing with Equation (9), magnitudes I_i and phases ϕ_i of the stator current $i_s(n)$ can be calculated as follows [27]:

$$I_i = |h_i|, I_i \in \mathbb{R},\tag{20}$$

$$\varphi_i = tg^{-1} \left[\frac{\operatorname{Im}(h_i)}{\operatorname{Re}(h_i)} \right], \, \phi_i \in \mathbb{R}. \tag{21}$$

Considering that the terms h_i and z_i appear in conjugate pairs, they indicate the presence of q/2 harmonics in the stator current signal. Hence, the performance of the root-Prony method is influenced by the model order q. In fact, a model order that is too high requires significant computing time, and in this case, the spectrum may include parasitic harmonics. Conversely, a model order that is too low risks missing low-order harmonics [8]. To estimate a suitable model order, several criteria have been developed [26, 30]. However, in this work, the stator current signal analysis is performed within a well-defined frequency band in which the fault-related harmonics are expected to appear. Therefore, the model order is fixed rather than estimated.

3.2 | Improved Root-Prony Method

The root-Prony method has significant drawbacks in terms of computation time, which increases with the number of samples in the analysed signal or with the model order. However, given that the sought fault signature can be found in a very specific region of the stator current spectrum, it is suggested to process the signal only within this specified frequency band. This approach, instead of sweeping the entire spectrum [8, 16], focuses solely on the components expected to characterise the fault. As a result, the length of the analysed spectrum is reduced, leading to lower computation time for the Root-Prony method to identify the desired fault. The following steps outline the procedure for inter-turn short circuits fault identification.

Step-1: Acquire the stator phase current

Step-2: Compute the phase current spectrum using fast Fourier transformation (FFT)

Step-3: Choose the appropriate frequency band $[f_b, f_h]$ for analysis, where f_b is the low cutoff and f_h is the high cutoff. This band, within the broader spectrum $[0, f_{\rm sf}/2]$, is selected

specifically to target the desired fault type. By narrowing the focus, the number of samples to process is reduced from N to $2N(f_h - f_b)/f_{\rm sf}$, resulting in substantial computational time savings.

Step-4: Apply the inverse FFT at the selected frequency band to obtain the appropriate time domain signal.

Step-5: Estimate signal parameters according to Equations (16), (17), (20) and (21). It should be noted that in this work, the frequency band used for identifying the stator ITSC fault is centred around the rotor slot harmonics.

4 | Application to Induction Motor Stator ITSC Fault Detection

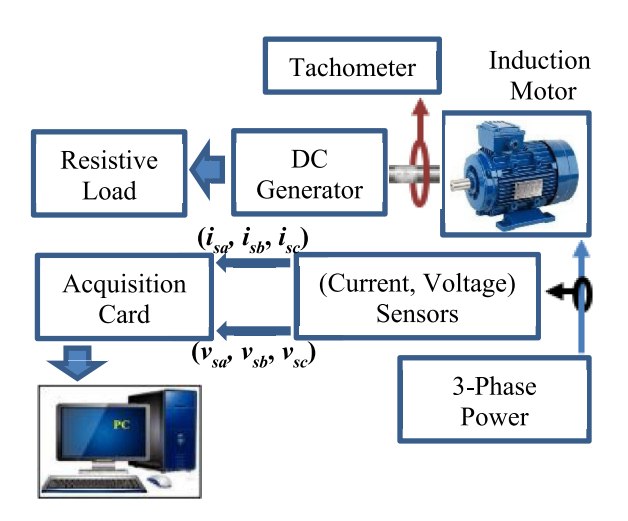
4.1 | Experimental Test Bench

A test bench was established at the Electrical Drive Development Laboratory (L.D.E.E-U.S.T.Oran) to experimentally validate the proposed method. This test bench comprises a 1.5 kW squirrel-cage IM, which utilises a single-layer lap winding with 4 coil groups per phase in a series connection. Each coil group consists of 3 identical coils, each with 18 turns. This IM is mechanically coupled to a DC generator with independent excitation, which supplies resistors acting as a variable resistive load to adjust the stator current. The technical specifications of the IM and generator are presented in the Appendix A. Furthermore, a data acquisition system and three Hall Effect sensors (Fluke i30s) were employed for current measurements. The entire system is shown in Figure 1. Acquisitions were performed under the steady-state condition of the IM's stator current, with the motor directly supplied by the three-phase power network. Each measurement was conducted over 10 s with a sampling frequency of 3 kHz, yielding a frequency resolution of 0.1 Hz. The motor's key parameters are 3.9 A, 1440 r. p.m., 10 Nm, 50 Hz, four poles, 36 stator slots and 44 rotor bars.

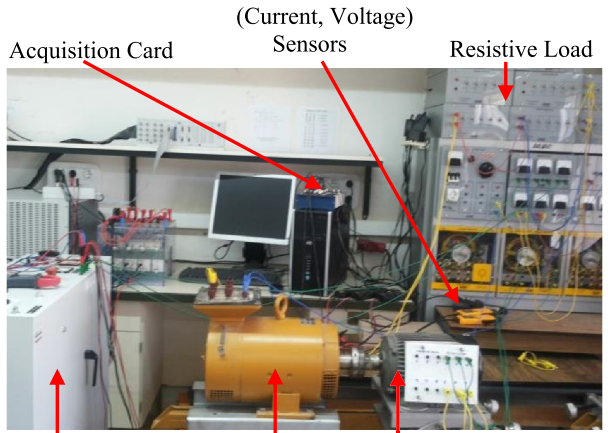
It should be emphasised that the proposed scheme is not strictly limited to a 3 kHz sampling frequency. This value was chosen as an optimal trade-off between frequency resolution and computational cost. A higher sampling frequency would slightly improve the resolution, but at the cost of a larger data size and higher computation time, whereas a lower sampling frequency could deteriorate the resolution around the rotor slot harmonics and compromise the accuracy of the root-Prony estimation. Consequently, the effectiveness of the proposed method is guaranteed as long as the chosen sampling rate offers sufficient resolution and ensures a reliable detection of the targeted harmonic components.

The IM was specifically wound to enable the generation of interturn short-circuit faults by incorporating multiple additional output points (see Figure 2 next page). These connections are located exclusively on phase 'a' of the stator, which allows for the simulation of realistic short-circuits. In practice, wires are soldered at various points of the winding and routed to a terminal plate. From the outside, it is thus very easy to locate the terminals, with each one identified by the number of turns to be

short-circuited. This setup provides access to 3 and 6 short-circuited turns, corresponding to 1.38% and 2.78% of the 216 turns in phase 'a', respectively. Consequently, a minimum of 16.66% of the turns in a coil can be short-circuited. In Figure 2, the rheostat R_f limits the short-circuit current. For further verification in this section, three operation modes, healthy, 3 ITSC and 6 ITSC, are used at different load torque values. The measurement of stator current with an inter-turn short circuit fault is performed as follows:



(a) High-level overview of the used setup.



3-Phases Supply DC Generator IM with accessible taps

(b) Photo of the used setup

FIGURE 1 | Experimental setup used in this work.

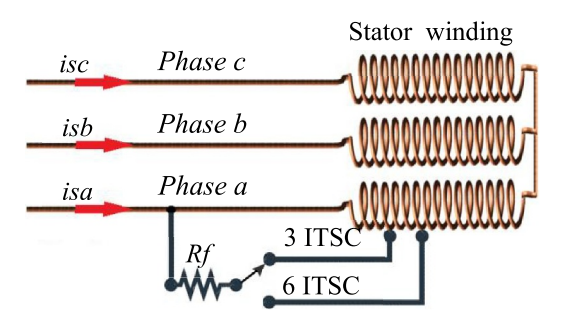


FIGURE 2 | Taps with shorted turns of a stator phase.

- Disconnect the induction motor from any supply source.
- Connect the short-circuit tap terminal to the input of the short-circuit rheostat. The output of the rheostat is then connected to the input of the phase.
- Connect the induction motor in a star (*Y*) configuration.
- Connect an ammeter in series between each motor phase and its corresponding electrical power supply terminal to measure the current.
- Assemble the separately excited generator and adjust its field current using the field rheostat to a specific value, in this case, 0.65 A.
- Start the induction motor without load, then gradually apply a load until the rated current of 3.9 A is reached.
- Adjust the short-circuit rheostat to ensure the current does not exceed 3.9 A.
- Position the three current sensors around each conductor to measure the current flowing through each specific motor phase. Each sensor end is connected to the data acquisition card. Similarly, place voltage sensors to measure the voltage on each motor phase, connecting their ends to the data acquisition card.
- At the computer level, adjust the sampling frequency and the acquisition duration.
- After each current and voltage measurement, perform data recording.

4.2 | The Analysed Frequency Band

It should be emphasised that the frequency bands analysed in this work are not chosen arbitrarily. Indeed, in the high-frequency region, the analysis is focused on the first rotor slot harmonics (RSH). To this end, it is first necessary to determine the frequency position of these harmonics, $f_{\rm L_RSH}$ and $f_{\rm U_RSH}$.

Accordingly, and based on the measured mechanical speed during the test, the slip values obtained in the healthy case, under no-load and full-load conditions, are 0.23% and 3.01%, respectively. By applying Equations (2) and (3), the theoretical rotor slot harmonic frequencies, $f_{\rm L_RSH}$ and $f_{\rm U_RSH}$, are then calculated and summarised in the following table:

Based on Table 2, it can be deduced that the necessary and sufficient frequency band for diagnosing this type of fault, by monitoring the evolution of the two frequencies sought, and more particularly of $f_{\rm L_RSH}$, can be limited to the interval [1010 Hz and 1150 Hz]. It should be noted that this band has been widened by \pm 5 Hz to account for variations in slip.

 $\textbf{TABLE 2} \quad | \quad \text{Theoretical frequencies of RSH-healthy case.}$

		Theoretical frequencies	
Tests types	S (%)	$f_{ extsf{L-RSH}}$	$f_{ extsf{U_RSH}}$
Without Load	0.23	1047.5 Hz	1147.5 Hz
Full load	3.01	1016.9 Hz	1116.9 Hz

4.3 | Induction Motor Stator Current Spectrum Periodogram Around the RSH

Figures 3–5 present the stator current spectra, generated via the periodogram method, highlighting the region around the rotor slot harmonics. These figures illustrate the differences in the spectrum for healthy, 3 ITSC and 6 ITSC stator fault conditions, under both no-load and full-load operation, respectively.

Figure 3 indicates that U_RSH is the only prominent component present in the healthy stator at both no-load and full-load conditions. However, the position of this harmonic component shifts to the left on the spectrum as the load increases. Conversely, the L RSH harmonic is difficult to discern.

A similar situation is also illustrated in Figure 4, which shows the presence of 3 ITSC faults. In this scenario, the L_RSH

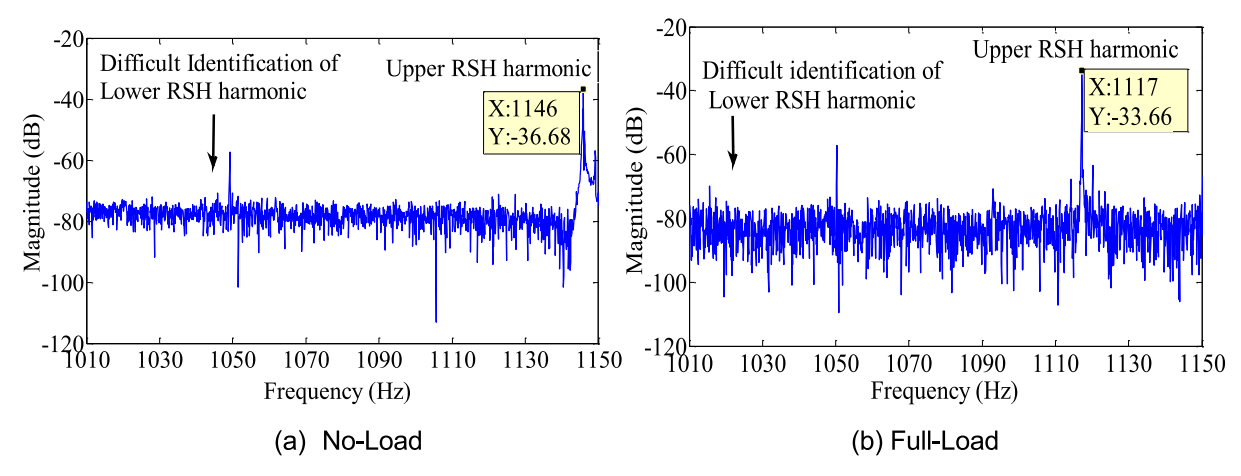


FIGURE 3 | Stator current spectrum: Healthy stator.

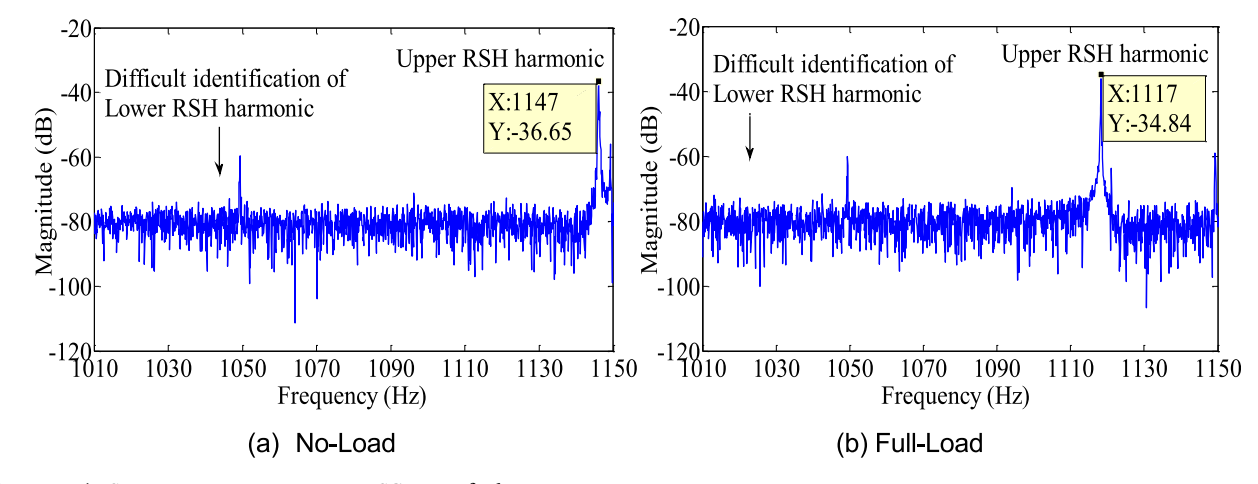


FIGURE 4 | Stator current spectrum: 3 ITSC stator fault.

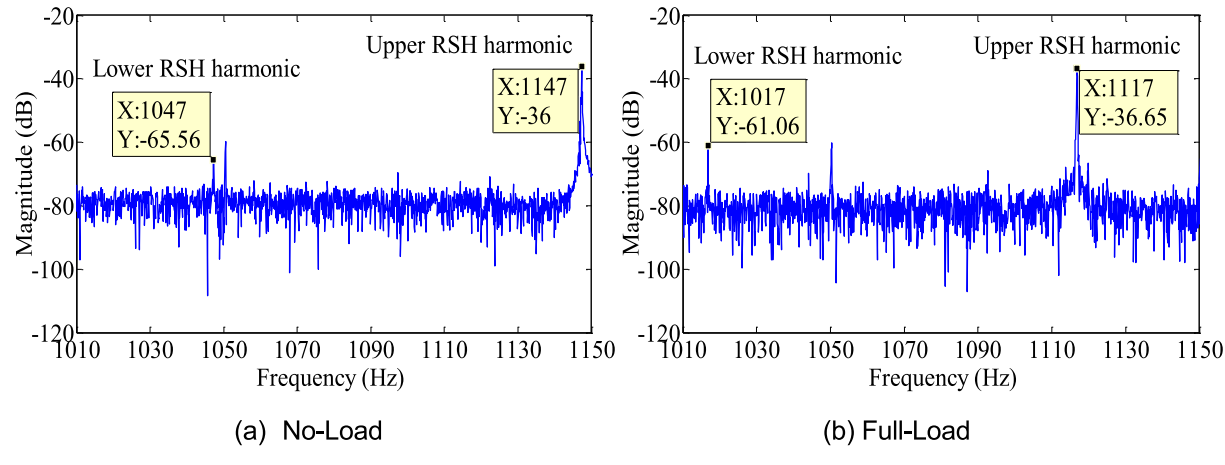


FIGURE 5 | Stator current spectrum—6 ITSC stator fault.

harmonic remains obscured by noise, even under high-load condition. Moreover, the magnitude of the U_RSH harmonic varies disproportionately with the load, making it difficult to utilise. In contrast, the L_RSH harmonic appears to be the sole reliable severity indicator for ITSC fault tracking. Figure 5 clearly shows the manifestation of the L_RSH harmonic component when the induction motor operates with a 6 ITSC faulty stator winding, at both no-load and full-load conditions. The magnitude of the U_RSH harmonic also varies slightly and disproportionately with the load, making it difficult to use. Therefore, the L_RSH harmonic can be considered as the most consistent indicator for tracking the ITSC fault. The experimental results confirm that this frequency band properly encompasses the evolution of the L_RSH harmonic, which proves to be the most reliable indicator for fault tracking.

4.4 \mid Application of Root-Prony Method to Stator Current

In this part, the root-Prony method is used to analyse the stator current signal. The stator current spectrum obtained using root-Prony is shown in Figure 6 (next page) in the case of no-load operation and in the absence of faults where the L_RSH

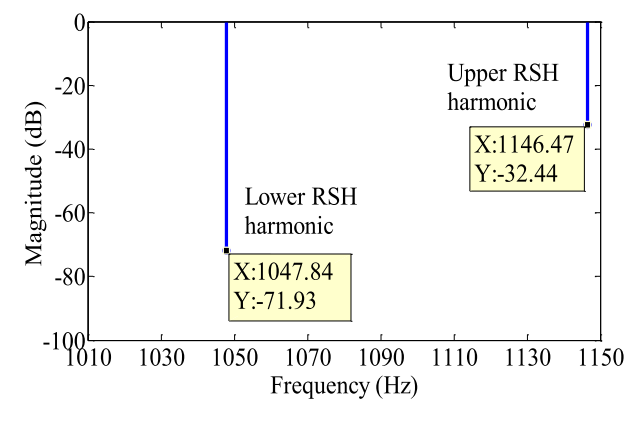


FIGURE 6 \mid Root-Prony stator current spectrum: Healthy case and no-load.

harmonic's magnitude is much lower and drowned in noise. It is noted that root-Prony method usage is considered satisfactory by the ability to extract such harmonic present at the frequency of 1047.84 Hz. The results in Table 3 showcase excellent frequency discrimination capabilities and a very good magnitude estimation of the L_RSH harmonic, considering both ITSC fault severity and varying load conditions when using the root-Prony technique. Specifically, for a given ITSC count, the magnitude of the L_RSH component decreases as the load value decreases. Conversely, under the same load condition, the L_RSH component's magnitude increases with an increasing ITSC count. Therefore, these findings demonstrate the superiority of root-Prony analysis over power spectral density by periodogram.

When the root-Prony method is applied, one can focus on a specific region of the signal, which allows for a more detailed analysis of that region. Therefore, after selecting the frequency band, the expression for the sampling frequency ($f_{\rm sf_RP}$) as well the corresponding frequency solution ($R_{\rm RP}$) can be written as follows:

$$f_{\rm sf_RP} = f_{\rm sf} \, \frac{N_{\rm RP}}{N},\tag{22}$$

$$R_{\rm RP} = \frac{f_{\rm sf_RP}}{N_{\rm RP}}.$$
 (23)

In our case, for example, the result is obtained in a time of 0.42 s, with an $N_{\rm RP}$ of 2800 samples and an $f_{\rm sf_RP}$ of 280 Hz. However, this does not directly change the frequency resolution, which remains equal to 0.1 Hz.

4.5 | Application of the Proposed Improved Root-Prony Method to Stator Current

• Computational Performance

To confirm the positive impact of the proposed solution in terms of computational performance, an experimental test was conducted. The results, presented in Table 4, include the

TABLE 3 | Estimating harmonics for stator phase currents' healthy and ITSC fault case by the root-Prony method.

			Tests type (load in %)	
Operating case	Harmonic	100%	50%	0%
Healthy stator	U_RSH	1117.27 Hz	1126.70 Hz	1146.47 Hz
		-33.63 dB	−34.17 dB	−32.44 dB
	L_RSH	1017.25 Hz	1026.91 Hz	1047.84 Hz
		-68.68 dB	−70.39 dB	−71.93 dB
3 ITSC	U_RSH	1115.88 Hz	1127.47 Hz	1146.57 Hz
		−34.73 dB	−34.22 dB	-33.64 dB
	L_RSH	1016.91 Hz	1026.51 Hz	1047.43 Hz
		−64.53 dB	−68.02 dB	−70.13 dB
6 ITSC	U_RSH	1116.91 Hz	1127.93 Hz	1147.04 Hz
		-32.50 dB	−35.93 dB	−34.54 dB
	L_RSH	1016.79 Hz	1026.25 Hz	1047.11 Hz
		−60.53 dB	−62.46 dB	−64.30 dB

computation time required for identifying only the fundamental frequency, the memory size used and the number of samples obtained using the improved root-Prony (RP) method. It is important to note that these results were obtained using a signal of 8192 samples with a sampling frequency of 3 kHz, resulting in a frequency resolution of 0.36 Hz. Furthermore, these tests were performed on a computer equipped with a dual-core processor running at 3.2 GHz and 4 GB of RAM.

• Performance Under Noisy Environment

In this operating mode, a speed controller is used in conjunction with the various elements present in the test bench depicted in Figure 1. The IM is powered through a two-level voltage source inverter. The DC power supply for the inverter is provided by a rectifier combined with an LC filter. The inverter's switches (comprised of transistors connected with anti-parallel diodes) receive their control signals from the sinusoidal pulse width modulation (SPWM) technique via an interface card. These signals enable the IM to be supplied with variable frequency voltages.

Stator current acquisitions were performed under steady-state operation of the induction motor, with the motor directly supplied by the inverter. Each measurement was carried out over 20 s with a sampling frequency of 3 kHz, yielding a frequency resolution of 0.05 Hz. These measurements will be useful to determine the impact of noise on the algorithm performance originating from the voltage source converter.

To illustrate this issue, we conducted two tests on an IM with a stator fault of 6 ITSC. The first test was performed at a supply frequency of 50 Hz, followed by the second test at a supply frequency of 30 Hz. This variation allows for increasing or decreasing the noise level in the IM's stator current signal.

For a power supply frequency of 50 Hz from the inverter, the measured mechanical speed during the first test resulted in a slip of 2.40%. For the second test, conducted with a power supply frequency of 30 Hz, the corresponding slip is 14.6%. Thus, based on Equations (2) and (3), the sought frequencies of the RSH, L_RSH and U_RSH are provided in Table 5.

The subsequent analysis in this section will focus solely on the L_RSH harmonic as the U_RSH harmonic was clearly visible in all previously illustrated cases. According to Figure 7, we can observe that the use of an inverter influences the temporal form of the stator current signal, making it less sinusoidal and more distorted due to the presence of ripples. These ripples can only be the manifestation of multiple coexisting harmonics, as clearly shown in Figure 8a, which represents the stator current

spectrum obtained by the periodogram method. Under inverter-fed conditions, the detection of the two desired harmonics, L_RSH and U_RSH, becomes particularly challenging due to the increased spectral distortion. This difficulty arises despite the fact that a 6 ITSC fault was easily identifiable when the IM was directly powered by the electrical grid.

Nevertheless, the improved RP method succeeds in isolating the L_RSH component, here identified at 1023.97 Hz, which closely matches the theoretical value reported in Table 5, thereby confirming its robustness under noisy operating conditions. This value is close to the calculated frequency mentioned in Table 5.

Figure 9a (next page) shows the results obtained using the classical PSD. We can observe that despite the decrease in the supply frequency to 30 Hz, and considering the stator fault at 6 ITSC, the identification of the L_RSH harmonic remains impossible. This demonstrates the influence of disturbances caused by the inverter on the stator current signal.

Figure 9b presents the desired harmonic in the specified frequency range using the proposed RP method. We can observe that this detected harmonic at 534.46 Hz accurately reflects the presence of a fault in the stator winding, aligning well with the frequency specified in Table 4.

The results obtained under the two power supply frequency conditions are summarised Table 6. From these results, it is observed that the fault frequency varies depending on the supply frequency. Therefore, if the temporal dimension of the spectrum is not considered, it becomes impossible to visualise this frequency variation, making fault detection unattainable. Furthermore, the proposed RP method can be successfully applied to different types of motors, provided it is adapted to the specific characteristics of the motor in question. However, it is important to note that the effectiveness of the RP method may vary depending on factors such as the nature of the faults present, the quality of the measurements and the availability of suitable data. Based on the analysis of the obtained results, it can be concluded that this method can be applied to real signals, subject to the following conditions:

 Accurately define the frequency range to be analysed where the desired fault is likely to occur. It is well known that

 $\textbf{TABLE 5} \quad | \quad \text{Theoretical frequencies of the sought harmonics.}$

	Computed		
Inverter supply	frequencies (Hz)		
frequency (Hz)	L_RSH	U_RSH	
50	1023.6	1123.6	
30	533.64	593.64	

TABLE 4 | Comparison of the root-Prony methods.

Method	Dl	Fundamental identification F (Hz)/A (dB)	MSU (Mbytes)	CT (s)
Original RP	8196	50.1/9.95	301	301
Improved RP	109	50.03/10.04	0.83	0.03

Abbreviations: CT, computation time; Dl, data length and MSU, memory size used.

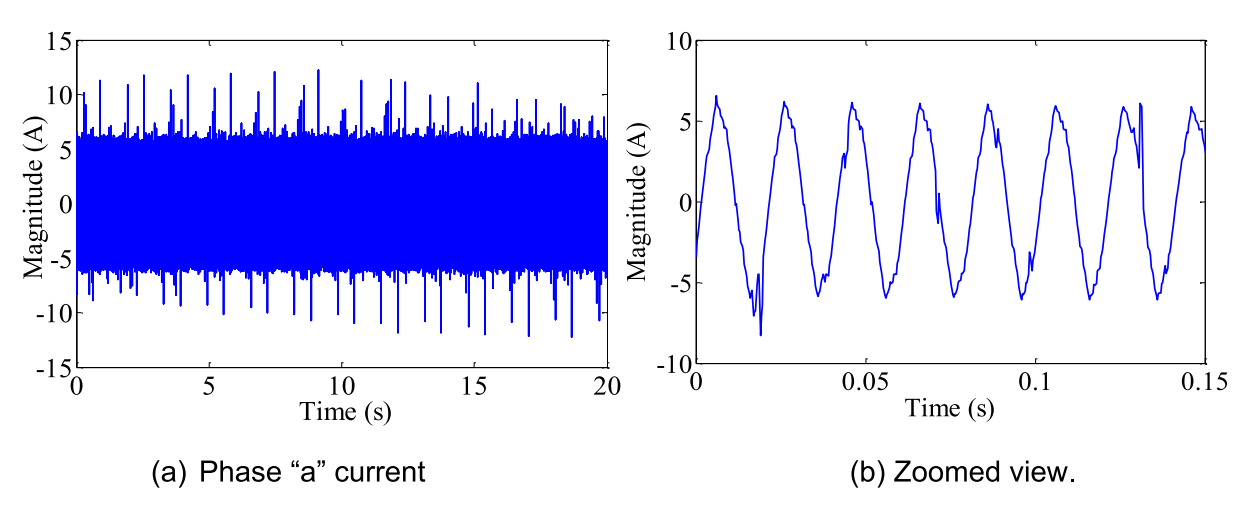


FIGURE 7 | Stator phase current of inverter-powered induction motor.

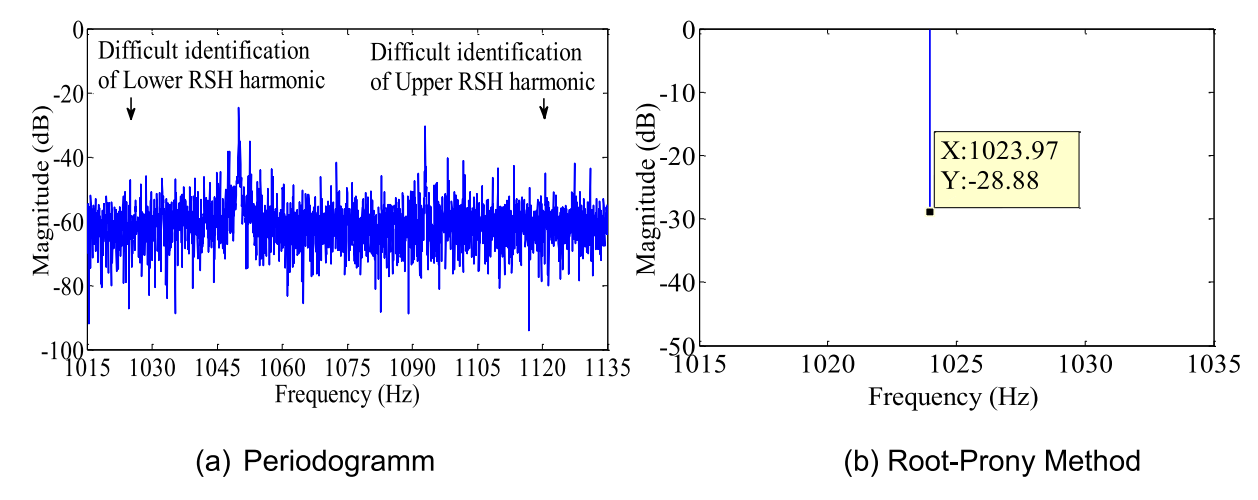


FIGURE 8 | Stator current spectrum: 6 ITSC fault stator and 50 Hz supply.

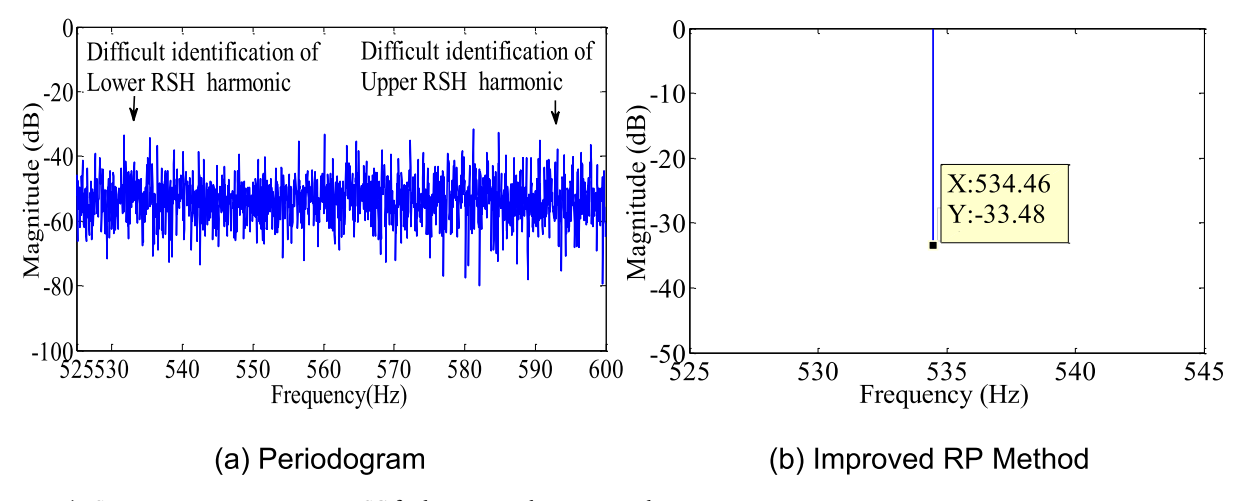


FIGURE 9 | Stator current spectrum: 6 ITSC fault stator and 30 Hz supply.

TABLE 6 | Performance and robustness of the improved RP method.

Supply (Hz)	Band	CT (s)	N_{RP}	f_{sf_RP}	R_{RP}
50	1015-1035	0.32	800	40	0.05
30	525-545	0.33	800	40	0.05

each fault has a specific signature located at a particular frequency.

• Ensure that the signal to be analysed does not have a high noise level. High noise can introduce random fluctuations into the signal, affecting detection accuracy and making pole representation very difficult. Indeed, this would

complicate the localisation of the signal's poles as they would be mixed with other poles representing the noise.

4.6 | Adaptability of the Diagnostic Scheme

• Robustness against inverter-related disturbances

The application of our method in a real industrial context, where machines are often powered by inverters, is a fundamental consideration. It is important to note that the proposed diagnostic scheme is conceived to remain independent of the inverter control strategy, focusing exclusively on fault-related harmonics.

This observation can be better understood by considering the effect of the PWM carrier frequency on the spectrum of stator currents. When a motor is supplied by an inverter, the PWM switching pattern introduces additional harmonics around multiples of the carrier frequency, which may complicate the spectrum [31]. However, these components are generally located in higher frequency bands than the fault-related harmonics of interest. Therefore, the root-Prony method, thanks to its parametric estimation capability, can reliably extract the fault signatures even in the presence of such disturbances.

• Applicability to nonstationary operating conditions

Furthermore, it is important to consider the impact of variations in speed and torque on the performance of the proposed scheme. Indeed, under varying load and speed conditions, the stator current spectrum becomes more complex due to the appearance of additional components. In this context, the proposed diagnostic scheme can be extended based on the principle of nonstationary analysis. Moreover, since the root-Prony approach can operate on well-defined time intervals, the signal can be divided into multiple segments, each of which can be analysed individually. This feature makes the approach particularly suitable for the analysis of nonstationary signals.

It is also important to note that in this study, the analysis was conducted under constant-speed operation, so the direct impact of speed variation was not considered. However, it should be noted that according to Equation (1), a change in speed (through slip variation) only shifts the exact frequency locations of the rotor slot harmonics without altering their diagnostic significance. In particular, the L_RSH remains a sensitive and reliable indicator of ITSC severity regardless of the operating point.

To provide clarification on our experimental approach, the following points are presented:

Experiments conducted under deliberately perturbed conditions, particularly with inverter-fed supply generating a spectrum rich in harmonics and high noise, demonstrated that the proposed improved root-Prony method preserves high frequency resolution and enables the isolation of the characteristic harmonic L_RSH. In this context, classical methods, such as the periodogram, failed to correctly

identify the fault components, highlighting the superiority of the proposed approach for processing noisy signals.

• Furthermore, the integration of torque as an input variable of the fuzzy system was carried out without the use of a dedicated sensor. The torque information was indirectly derived from the loading conditions, providing an estimation sufficiently accurate for the implementation of the method. This strategy avoids the need for costly and potentially cumbersome sensors while ensuring a reliable representation of the applied load.

5 | Integration of Fuzzy Logic Monitoring System

The work presented in this section is based on the application of fuzzy logic to diagnose induction motor stator winding faults [32–36]. According to the obtained experimental results, the L_RSH harmonic is particularly sensitive to fault severity; thus, this harmonic's magnitude is considered a parameter to characterise the fault's evolution.

It should be noted that fault severity is directly related to load variation. As the load value increases, the magnitude of L_RSH also increases and vice versa. Therefore, to track the motor's state, the fuzzy logic system takes two inputs: the magnitude of the L_RSH component (Acc) and the load torque value (Ld). Based on these inputs and defined rules, the inference system determines the nature of the stator's state, specifically, whether it is healthy or has an inter-turn short-circuit fault. The suggested approach to identifying the stator state is illustrated in Figure 10.

5.1 | Fuzzy System Input-Output Variables

The fuzzy logic system is based on fuzzy rules and membership functions that can be formed by a set of data represented as linguistic variables. Figure 11 shows the membership functions for the different input variables. The Acc and Ld inputs are as follows:

- T (Acc) = {VS, S, M, L}. Where, VS (very small), S (small), M (medium) and L (large).
- T (Ld) = {LL, AL, HL} with, LL (low load), AL (average load) and HL (high load).

For the output SC (stator condition) of the fuzzy system, which identifies the stator state, it is defined by the set $T(SC) = \{HH, F, SF\}$. Here, HH can be interpreted as a motor without fault, F

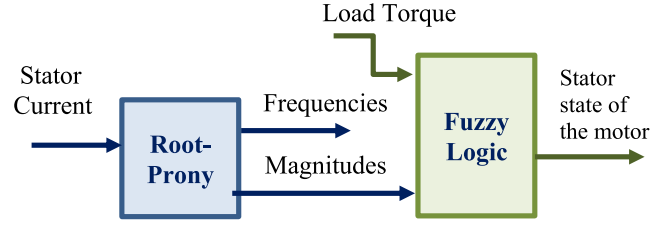


FIGURE 10 | Stator fault diagnosis using fuzzy logic.

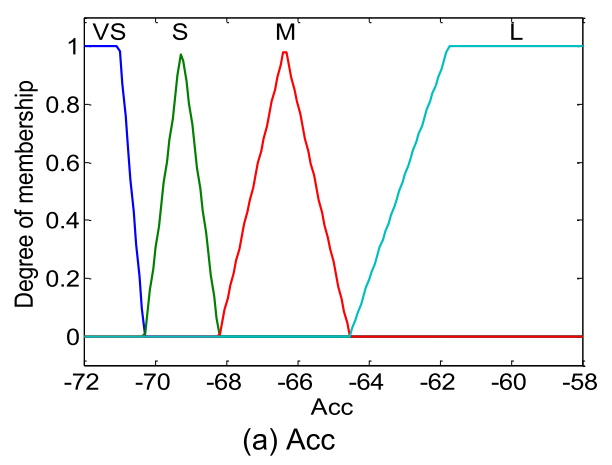


FIGURE 11 | Membership functions for the Acc and Ld inputs.

as a 3 ITSC fault in the stator winding and similarly, SF as a 6 ITSC fault. Table 7 describes the output ranges for these output variables.

5.2 | Fuzzy Rule Base

- 1. If (Acc is VS) and (Ld is LL) then (SC is HH)
- 2. If (Acc is VS) and (Ld is AL) then (SC is HH)
- 3. If (Acc is VS) and (Ld is HL) then (SC is HH)
- 4. If (Acc is S) and (Ld is LL) then (SC is F)
- 5. If (Acc is S) and (Ld is AL) then (SC is HH)
- 6. If (Acc is S) and (Ld is HL) then (SC is HH)
- 7. If (Acc is M) and (Ld is LL) then (SC is F)
- 8. If (Acc is M) and (Ld is AL) then (SC is F)
- 9. If (Acc is M) and (Ld is HL) then (SC is F)
- 10. If (Acc is L) and (Ld is LL) then (SC is SF)
- 11. If (Acc is L) and (Ld is AL) then (SC is SF)
- 12. If (Acc is L) and (Ld is HL) then (SC is SF)

Figure 12 shows the structure of the proposed fuzzy logic-based supervisory system, which infers the stator condition using a Mamdani-type inference system. The defuzzification process applies the centroid method.

5.3 | Results of the Fuzzy Logic Diagnostic System

To validate the fuzzy logic diagnostic system's performance, tests were carried out under different load torque values for both a healthy stator winding and one with an ITSC fault. Table 8 presents the results obtained by applying the proposed root-Prony method to the stator current. Subsequently, to evaluate the inputs and determine the stator state, the L_RSH component magnitude and the load conditions are introduced into the fuzzy system. The L_RSH harmonic magnitudes for different stator conditions under 75% and 25% load are summarised in Table 8.

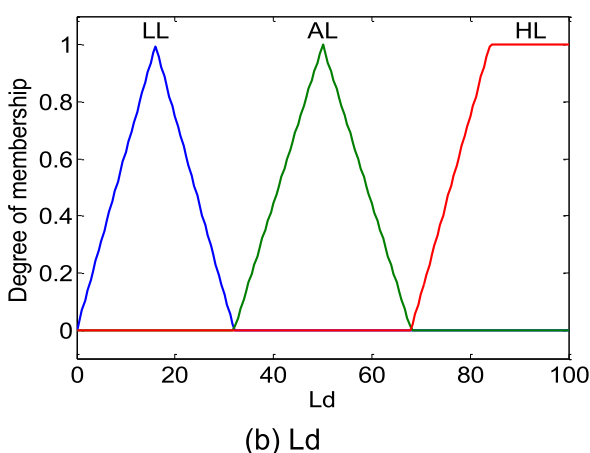


TABLE 7 | Range of outputs variables.

Range	Stator condition	Number of stator ITSC
$0 \le \text{output} \le 0.3$	Health (HH)	0
$0.31 \le \text{output} \le 0.6$	Fault (F)	3
$0.61 \le \text{output} \le 1$	Severe fault (SF)	6

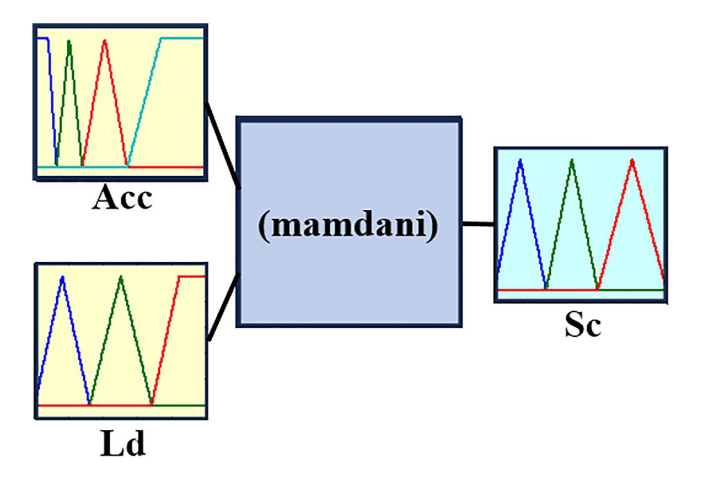


FIGURE 12 | Proposed fuzzy logic supervisory system.

The numerical values of the SC output obtained by the fuzzy diagnostic system, presented in Tables 9–11, indicate that, according to Table 3, the state of the stator winding is healthy, with a 3 ITSC fault and with a 6 ITSC fault, respectively.

As shown in Table 3 and the findings in Tables 9–11, the fuzzy logic system is able to distinguish between the healthy condition and stator faults caused by 3 and 6 ITSCs. Therefore, the number of shorted turns is correctly determined.

6 | Conclusion and Future Works

In this article, a technique using the fuzzy logic approach was presented and tested to improve the ability to diagnose interturn short-circuit faults in an induction motor stator. For this purpose, an improved root-Prony method was applied to

TABLE 8 | L_RSH harmonic's estimation by the proposed root-Prony method in the two cases, healthy and ITSC fault of a stator phase (75% and 25% of load).

State of stator	Healthy	3 turns shorted	6 turns shorted	Load (%)
L_RSH harmonic	1020.89 Hz	1020.61 Hz	1020.03 Hz	75
	−69.47 dB	−65.31 dB	−61.21 dB	
	1032.05 Hz	1031.91 Hz	1031.37 Hz	25
	−70.93 dB	−69.32 dB	−63.17 dB	

TABLE 9 | Results of the fuzzy system—healthy stator.

Inputs		Output
Acc (dB)	Ld (%)	sc
-70.93	25	0.15
-70.39	50	0.15
-69.47	75	0.15

TABLE 10 | Results of the fuzzy system—stator with 3 ITSC fault.

Inputs		Output
Acc (dB)	Ld (%)	sc
-69.32	25	0.45
-68.02	50	0.45
-65.31	75	0.45

TABLE 11 | Results of the fuzzy system—stator with 6 ITSC fault.

Inputs		Output
Acc (dB)	Ld (%)	sc
-63.17	25	0.8
-62.46	50	0.8
-61.31	75	0.8

estimate the magnitude of the fault harmonics, particularly the low-magnitude harmonics, around the rotor slot harmonics at different load torque values. These magnitudes, along with the load applied to the motor, are considered inputs to the fuzzy diagnostic system. The system's output represents the stator winding state. Different loads and ITSC fault values were applied to the system during testing. The results demonstrate the system's capability for detecting the fault and determining the ITSC number.

However, although the results obtained are conclusive, further research is needed to explore the challenges raised in this study, including:

- Extend the proposed diagnostic scheme for nonstationary signal analysis, in order to allow fault detection under variable speed and/or load conditions.
- Explore the impact of the Park transformation on the detection of inter-turn short circuit faults and study ways to overcome the disadvantages of this approach.

 Integrate a dedicated torque sensor to validate the accuracy of the torque estimation used in this study and evaluate its impact on diagnostic performance.

Author Contributions

Mohamed Kouadria: conceptualization, formal analysis, investigation, methodology, validation, visualization, writing – original draft. Ahmed Zakaria Mehdi Chedjara: conceptualization, formal analysis, writing – review and editing. Hafiz Ahmed: conceptualization, formal analysis, writing – review and editing. Chun-Lien Su: supervision, writing – review and editing. Mohamed Benbouzid: supervision, writing – review and editing. Josep M. Guerrero: supervision, writing – review and editing.

Acknowledgements

Declaration of Generative AI and AI-Assisted Technologies in the Writing Process: During the preparation of this work, the authors used ChatGPT exclusively to assist with language refinement and readability. All AI-generated content was carefully reviewed, edited and verified by the authors, who take full responsibility for the accuracy, integrity and originality of the final manuscript.

Funding

The authors have nothing to report.

Conflicts of Interest

The authors declare no conflicts of interest.

Data Availability Statement

The data that have been used are confidential.

References

- 1. J. Herrera-Guachamin, J. Antonino-Daviu, "Laboratory Experiments for the Evaluation of the Efficiency of Induction Motors Operating Under Different Electrical and Mechanical Faults," in *IECON* 2019—45th Annual Conference of the IEEE Industrial Electronics Society, (2019), 6319–6322, https://doi.org/10.1109/IECON.2019.8927328.
- 2. T. Garcia-Calva, D. Morinigo-Sotelo, V. Fernandez-Cavero, and R. Romero-Troncoso, "Early Detection of Faults in Induction Motors—A Review," *Energies* 15, no. 21 (2022): 7855, https://doi.org/10.3390/en15217855.
- 3. P. Rodriguez, S. Sahoo, C. T. Pinto, and M. Sulowicz, "Field Current Signature Analysis for Fault Detection in Synchronous Motors," in 2015 IEEE 10th International Symposium on Diagnostics for Electrical Machines, Power Electronics and Drives (SDEMPED), (2015), 246–252, https://doi.org/10.1109/DEMPED.2015.7303697.
- 4. F. B. Batista, P. C. M. Lamim Filho, R. Pederiva, and V. A. D. Silva, "An Empirical Demodulation for Electrical Fault Detection in Induction

- Motors," *IEEE Transactions on Instrumentation and Measurement* 65, no. 3 (March 2016): 559–569, https://doi.org/10.1109/tim.2015.2509398.
- 5. A. Rassõlkin, A. Kallaste, S. Orlova, L. Gevorkov, T. Vaimann, and A. Belahcen, "Re-Use and Recycling of Different Electrical Machines," *Latvian Journal of Physics and Technical Sciences* 55, no. 4 (2018): 13–23, https://doi.org/10.2478/lpts-2018-0025.
- 6. N. Bhole and S. Ghodke, "Motor Current Signature Analysis for Fault Detection of Induction Machine-A Review," in 2021 4th Biennial International Conference on Nascent Technologies in Engineering (ICNTE), (2021), 1–6, https://doi.org/10.1109/ICNTE51185.2021.9487715.
- 7. P. Dong, S. Yang, H. Yang, Q. Wang, and M. Li, "High Efficient and Real-Time Realization of Zoom FFT Based on FPGA," in 2010 International Conference on Computer Application and System Modeling (ICCASM 2010), (2010) V2-669-V2-673, https://doi.org/10.1109/ICCASM.2010.5620514.
- 8. A. H. Boudinar, N. Benouzza, A. Bendiabdellah, and M.-E.-A. Khodja, "Induction Motor Bearing Fault Analysis Using a Root-MUSIC Method," *IEEE Transactions on Industry Applications* 52, no. 5 (September/October 2016): 3851–3860, https://doi.org/10.1109/TIA. 2016.2581143.
- 9. A. Boudinar, A. F. Aimer, M.-El-A. Khodja, B. Noureddine, "Induction Motor's Bearing Fault Diagnosis Using an Improved Short Time Fourier Transform," in *Advanced Control Engineering Methods in Electrical Engineering Systems*, (January 2019), 411–426, https://doi.org/10.1007/978-3-319-97816-1_31.
- 10. G. Tarchała, M. Wolkiewicz, and M. Krzysztofiak, "Diagnosis of Short-Circuits in Induction Motor Stator Winding Using a Modified Park Transformation," *Power Electronics and Drives* 5, no. 41 (2020): 123–133, https://doi.org/10.2478/pead-2020-0009.
- 11. S. H. Kia, H. Henao, and G.-A. Capolino, "Zoom-MUSIC Frequency Estimation Method for Three-Phase Induction Machine Fault Detection," in 31st Annual Conference of IEEE Industrial Electronics Society, 2005. IECON 2005, (2005), https://doi.org/10.1109/IECON. 2005.1569317.
- 12. A. Garcia-Perez, R. d. J. Romero-Troncoso, E. Cabal-Yepez, and R. A. Osornio-Rios, "The Application of High-Resolution Spectral Analysis for Identifying Multiple Combined Faults in Induction Motors," *IEEE Transactions on Industrial Electronics* 58, no. 5 (May 2011): 2002–2010, https://doi.org/10.1109/TIE.2010.2051398.
- 13. B. Xu, L. Sun, L. Xu, and G. Xu, "An ESPRIT-SAA-Based Detection Method for Broken Rotor Bar Fault in Induction Motors," *IEEE Transactions on Energy Conversion* 27, no. 3 (September 2012): 654–660, https://doi.org/10.1109/TEC.2012.2194148.
- 14. K. C. Deekshit Kompella and G. V. Madhav, "An Improved Matrix Pencil Method Based Bearing Fault Detection in Three Phase Induction Motor," in 2020 IEEE International Conference on Computing, Power and Communication Technologies (GUCON), Greater Noida, (2020), 51–56, https://doi.org/10.1109/GUCON48875.2020.9231196.
- 15. M. Kouadria, Z. Chedjara, C. Su, et al., "Diagnosis of Induction Motor Stator Faults Around Rotor Slot Harmonics Using the Matrix Pencil Method", *Results in Engineering* 25 (2025), 104240 ISSN 2590–1230, https://doi.org/10.1016/j.rineng.2025.104240.
- 16. M. Kouadria, A. H. Boudinar, A. Bendiabdellah, and N. Benouzza, "Induction Motor Stator Fault Diagnosis by Rotor Slots Harmonics Tracking Using Prony Improved Approach," *International Review of Automatic Control* 10, no. 4 (2017): 1974–6059, https://doi.org/10.15866/ireaco.v10i4.11880.
- 17. L. A. T. Guajardo, M. A. P. Garza, J. R. Maldonado, M. A. G. Vázquez, L. H. R. Alfaro, and F. S. Salinas, "Prony Method Estimation for Motor Current Signal Analysis Diagnostics in Rotor Cage Induction Motors," *Energies* 15, no. 10 (2022): 3513, https://doi.org/10.3390/en15103513.

- 18. M. Kouadria, Z. Chedjara, M. Benbouzid, et al., "A Zoomed Root-Prony Technique for Efficient Bearing Fault Detection in Induction Motors," *Results in Engineering* 24 (2024): 103367, https://doi.org/10.1016/j.rineng.2024.103367.
- 19. S. Das, P. Purkait, and S. Chakravorti, "Separating Induction Motor Current Signature for Stator Winding Faults From That Due To Supply Voltage Unbalances," in 2012 1st International Conference on Power and Energy in NERIST (ICPEN), (2012), 1–6, https://doi.org/10.1109/ICPEN. 2012.6492315.
- 20. A. Khechekhouche, H. Cherif, A. Menacer, S. E. Chehaidia, and H. Panchal, "Experimental Diagnosis of Inter-Turns Stator Fault and Unbalanced Voltage Supply in Induction Motor Using MCSA and DWER," *Periodicals of Engineering and Natural Sciences* 8, no. 3 (2020): 1202–1216, https://doi.org/10.21533/pen.v8.i3.1159.
- 21. J. Faiz, V. Ghorbanian, and G. Joksimović, *Fault Diagnosis of Induction Motors*. 1st ed. (Institution of Engineering and Technology (IET), 2017), https://doi.org/10.1049/PBPO108E.
- 22. G. M. Joksimovic and J. Penman, "The Detection of Inter-Turn Short Circuits in the Stator Windings of Operating Motors," *IEEE Transactions on Industrial Electronics* 47, no. 5 (October 2000): 1078–1084, https://doi.org/10.1109/41.873216.
- 23. A. Khezzar, M. Y. Kaikaa, M. E. K. Oumaamar, M. Boucherma, and H. Razik, "On the Use of Slot Harmonics as a Potential Indicator of Rotor Bar Breakage in the Induction Machine," *IEEE Transactions on Industrial Electronics* 56, no. 11 (November 2009): 4592–4605, https://doi.org/10.1109/TIE.2009.2030819.
- 24. S. Nandi and H. A. Toliyat, "Novel Frequency-Domain-Based Technique to Detect Stator Interturn Faults in Induction Machines Using Stator-Induced Voltages After Switch-Off," *IEEE Transactions on Industry Applications* 38, no. 1 (January/February 2002): 101–109, https://doi.org/10.1109/28.980363.
- 25. A. F. Aimer, A. H. Boudinar, M. E. A. Khodja, and A. Bendiabdellah, "Monitoring and Fault Diagnosis of Induction Motors Mechanical Faults Using a Modified Auto-Regressive Approach," in *Advanced Control Engineering Methods in Electrical Engineering Systems* (Springer International Publishing, 2018), 390–410, https://doi.org/10.1007/978-3-319-97816-1_30.
- 26. Y.-H. Kim, Y.-W. Youn, D.-H. Hwang, J.-H. Sun, and D.-S. Kang, "High-Resolution Parameter Estimation Method to Identify Broken Rotor Bar Faults in Induction Motors," *IEEE Transactions on Industrial Electronics* 60, no. 9 (September 2013): 4103–4117, https://doi.org/10.1109/TIE.2012.2227912.
- 27. S. Chen and R. Zivanovic, "Estimation of Frequency Components in Stator Current for the Detection of Broken Rotor Bars in Induction Machines," *Measurement: Journal of the International Measurement Confederation* 43, no. 7 (2010): 887–900, https://doi.org/10.1016/j.measurement.2010.03.006.
- 28. M. H. Hayes, Statistical Digital Signal Processing and Modelling (John Wiley & Sons, Inc, 1991).
- 29. T. JinRui, Y. XiangGen, Z. Zhe, H. ZhiQin, Y. Lei, and W. Yuxue, "Fault Location in Distribution Networks Using Prony Analysis," in 2011 Advanced Power System Automation and Protection Conference, (2011), 54–59, https://doi.org/10.1109/APAP.2011.6180384.
- 30. F. Cong, A. K. Nandi, Z. He, A. Cichocki, and T. Ristaniemi, "Fast and Effective Model Order Selection Method to Determine the Number of Sources in a Linear Transformation Model," in *Proceedings of the 20th European Signal Processing Conference (EUSIPCO)*, (2012), 1870–1874.
- 31. J. Tang, Y. Yang, J. Chen, R. Qiu, and Z. Liu, "Characteristics Analysis and Measurement of Inverter-Fed Induction Motors for Stator and Rotor Fault Detection," *Energies* 13, no. 1 (2020): 1–17 Article 101, https://doi.org/10.3390/en13010101.
- 32. S. S. Shetgaonkar, "Fault Diagnosis in Induction Motor Using Fuzzy Logic," in 2017 International Conference on Computing Methodologies

and Communication (ICCMC), (2017), 289–293, https://doi.org/10.1109/ICCMC.2017.8282693.

- 33. O. R. Agyare, A. B. Asiedu-Asante, and A. R. Biney, "Fuzzy Logic Based Condition Monitoring of a 3-Phase Induction Motor," in *2019 IEEE AFRICON* (2019), 1–8, https://doi.org/10.1109/AFRICON46755. 2019.9133780.
- 34. V. R. Metha and S. S. Karvekar, "Speed Control of Induction Motor Using A Fuzzy Logic Controller and Direct Torque Controller," in *2018 4th International Conference for Convergence in Technology (I2CT)*, (2018), 1–5, https://doi.org/10.1109/I2CT42659.2018.9058085.
- 35. G. J. Naveena, M. Dodakundi, and A. Layadgundi, "Fault Diagnosis of VSI Fed Induction Motor Drive Using Fuzzy Logic Approach," in 2015 International Conference on Power and Advanced Control Engineering (ICPACE), (2015), 315–321, https://doi.org/10.1109/ICPACE. 2015.7274965.
- 36. P. Thejasree, N. Manikandan, N. Sunheriya, et al., "Development of an Artificial Intelligence Model for Wire Electrical Discharge Machining of Inconel 625 in Biomedical Applications," *IET Collaborative Intelligent Manufacturing* 6, no. 4 (December 2024): e70015, https://doi.org/10.1049/cim2.70015.

Appendix A

Parameters of the induction motor	
Rated power (kW)	1.5
Winding connection	Y
Supply frequency (Hz)	50
Rated voltage (V)	380
Rated current rotor (A)	3.9
Rated speed (r.p.m.)	1440
Number of rotor bars	44
Number of stator slots	36
Stator turns per phase	216
Number of pair of poles	2
Parameters of the DC generator	
Rated power (kW)	2.4
Armature voltage (V)	220
Armature current (A)	10.9
Excitation current (A)	0.65
Rated speed (r.p.m.)	1410
Excitation type	Separate